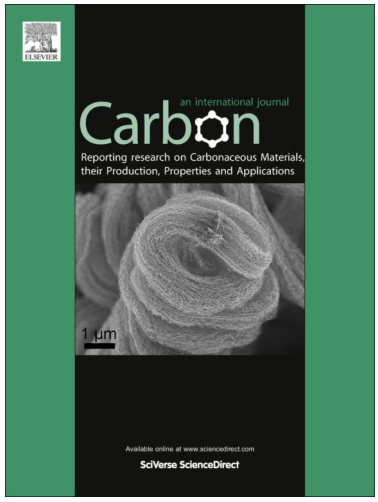

High-yield exfoliation of graphite in acrylate polymers: a stable few-layer graphene nanofluid with enhanced thermal conductivity

Zhenyu Sun, Sascha Pöller, Xing Huang, Dmitrii Guschin, Christoph Taetz, Petra Ebbinghaus, Justus Masa, Andreas Erbe, Andreas Kilzer, Wolfgang Schuhmann, Martin Muhler

PII: S0008-6223(13)00697-0
DOI: http://dx.doi.org/10.1016/j.carbon.2013.07.063
Reference: CARBON 8244

To appear in: *Carbon*

Received Date: 2 April 2013
Accepted Date: 21 July 2013

Please cite this article as: Sun, Z., Pöller, S., Huang, X., Guschin, D., Taetz, C., Ebbinghaus, P., Masa, J., Erbe, A., Kilzer, A., Schuhmann, W., Muhler, M., High-yield exfoliation of graphite in acrylate polymers: a stable few-layer graphene nanofluid with enhanced thermal conductivity, *Carbon* (2013), doi: http://dx.doi.org/10.1016/j.carbon.2013.07.063

High-yield exfoliation of graphite in acrylate polymers: A stable few-layer graphene nanofluid with enhanced thermal conductivity

Zhenyu Sun,[a] Sascha Pöller,[b] Xing Huang,[c] Dmitrii Guschin,[b] Christoph Taetz,[d] Petra Ebbinghaus,[e] Justus Masa,[b] Andreas Erbe,[e] Andreas Kilzer,[d] Wolfgang Schuhmann,[b] and Martin Muhler[a]

[a] *Laboratory of Industrial Chemistry, Ruhr-University Bochum, D-44780, Bochum, Germany.*

[b] *Analytische Chemie-Elektroanalytik & Sensorik, Ruhr-University Bochum, D-44780, Bochum, Germany*

[c] *Institute of Physics and Chemistry, Chinese Academy of Sciences, Beijing, China*

[d] *Lehrstuhl für verfahrenstechnische Transportprozesse, Ruhr-University Bochum, D-44780, Bochum, Germany*

[e] *Max-Planck-Institut für Eisenforschung GmbH, Max-Planck-Str. 1, 40237 Düsseldorf, Germany*

High-yield exfoliation of pristine graphite in low boiling point alcohols was achieved using a set of acrylate polymers resulting in few-layer graphene concentrations of up to ~4 mg mL^{-1}. The polymer showed superior dispersing capabilities for graphene compared to the best reported dispersants, including the solvent *N*-methyl-pyrrolidone, the surfactants sodium cholate and sodium taurodeoxycholate, and the polymer polyvinylpyrrolidone. The dispersions were stable regardless of freezing (-26 °C) or heating (70 °C) for 24 h, or dilution with water up to 80%

Corresponding author: Tel.: +49 234 32-24518.

E-mail address: zhenyu.sun@techem.rub.de (Z.Y. Sun).

volume ratio over 160 h. The as-obtained nanofluid exhibited an enhancement in thermal conductivity suggesting a great potential in coolant applications.

1. Introduction

Two-dimensional atomic crystals have recently become a subject of intense research as building blocks for a range of functional architectures [1]. Graphene (G) is likely the best known two-dimensional material owing to its unique combination of electronic, thermal, and mechanical properties. Carrier mobilities as high as 200, 000 cm^2 V^{-1} s^{-1}, thermal conductivities up to 5000 W mK^{-1} and Young's moduli of 0.5-1 TPa have been reported [2]. For practical applications and to facilitate processing, producing graphene in large quantities is a prerequisite. Currently, the most commonly used approach involves the oxidation of graphite, followed by exfoliation in water or organic solvents to yield graphene oxide (GO) [3]. Subsequent chemical or thermal reduction is essential to remove epoxy, carboxy, or hydroxy groups, which complicates the processing [4]. Whilst post-treatment enables GO to partly regain its electrical conductivity, many defects in the sp^2 carbon lattice that were introduced during the oxidation process cannot be fully reversed by reduction, thus leading to undesirable degradation of the intrinsic performance of graphene. In addition to tedious multistep processes, this method also involves the use of hazardous oxidizing (e.g., HNO_3, H_2SO_4, $KMnO_4$) and reducing (e.g., hydrazine, $NaBH_4$) reagents causing environmental issues as well as safety concerns.

One potential pathway for addressing these issues is to exfoliate graphene directly from pristine graphite in the liquid phase, using protocols analogous to those developed in the context of the chemistry of fullerenes and carbon nanotubes (CNTs) [5]. This can typically be achieved by exfoliation of layered graphite via ultrasonication in an appropriate liquid [6]. The exfoliated sheets can be stabilized noncovalently against re-aggregation by interaction with certain solvents

[6-8], surfactants [9-11], polymers [12], or aromatic π-π stacking molecules [13-15]. This top-down approach has aesthetic appeal due to its simplicity, low cost, and flexibility in manipulating graphene into various processes, such as blending, casting, or functionalization. Importantly, the stabilization is based on van der Waals interactions between the sheets and the stabilizer molecules such that the properties of graphene are preserved.

Despite recent advances in this field, the exfoliation of graphene can only be achieved in a very limited number of systems and suffers from drawbacks such as relatively low concentrations and the need for extensive sonication. It is of great significance to discover new agents for dispersing graphene at reasonably high concentrations especially in low boiling point solvents, and also to develop efficient processes to enhance the yield of graphene. Herein, we demonstrate a set of acrylate polymers that can effectively exfoliate and stabilize pristine graphene in both ethanol (EtOH) and isopropanol (*i*-PrOH). The chemical structures and synthesis procedures of the polymers are shown in the Supporting Information. As far as we are aware, very few studies in literature have used acrylate polymers for direct exfoliation of graphite to pristine graphene. Previous work mainly reported an enhancement in the colloidal stability of GO and reduced GO dispersions via polyacrylate coating and fabrication of GO or reduced GO/acrylate polymer composites [16-18]. Here, stable graphene dispersions in ethanol were produced with concentrations up to ~4 mg mL^{-1} using the polymer poly (co-(*n*-butyl acrylate)-co-(allyl methacrylate)-co-(poly-(ethylene glycol) methacrylate) (P20). The polymer showed superior dispersing capabilities for graphene compared to the best reported dispersants, including the solvent *N*-methyl-pyrrolidone (NMP) [6-7], the surfactants sodium cholate (SC) [10] and sodium taurodeoxycholate (STC) [11], and the polymer polyvinylpyrrolidone (PVP) [12], in terms of the absorbance per unit-cell-length at 660 nm (A_{660}/l) under identical experimental conditions.

2. Experimental

2.1 Materials All chemicals used in this work were of analytical grade and used as supplied. N-Methyl-2-pyrrolidinone (product number 270458), anionic surfactants sodium taurodeoxycholate (product number T0875) and sodium cholate (product number C1254) and polyvinylpyrrolidone (product number 856568) were purchased from Sigma-Aldrich. Graphite powder (product number 332461) was also acquired from Sigma-Aldrich and used without further treatments.

2.2 Synthesis of the polymers P20, P08, and P19 Polymerization was carried out as described in our previous work [19]. The amounts of the monomers of polyethylene glycol methacrylate (PEGMA), allyl methacrylate (AllMA), butyl acrylate (BA), 2-(dimethylamino) ethyl methacrylate (DMAEMA) and methacrylic acid (MAA) used for the synthesis of the polymers are shown in Table S1. Excess monomers were removed by precipitation. Polymers P19 and P20 were precipitated from water, separated by centrifugation (3500 rpm, 10 min), re-dissolved in *i*-PrOH (5.0 mL) and neutralised (P19: 10 M KOH_{aq}, 20 µL; P20: 10 M KOH_{aq}, 40 µL) to give the final polymer suspensions (P19: 4.7% w/w; P20: 2.5% w/w). The polymer P08 was neutralised using HCl_{aq} (10 M, 0.24 mL), precipitated from H_2O by shifting the pH value to basic range using KOH (10 M) and re-dissolved in water by shifting the pH value back to acidic state using HCl (10 M). This was repeated three times and the final polymer was dissolved in EtOH (2.0 mL) and neutralised using HCl_{aq} (10 M, 0.24 mL), to give the final polymer suspension (P08: 5.7% w/w). Following a similar procedure, P20 suspensions with a higher weight concentration of 10.0% w/w were obtained by use of 200 mmol of monomers, which were diluted for polymer concentration investigation.

2.3 Polymer exfoliation of graphene Typically, graphene dispersions were prepared by adding graphite to 2.5 mL polymer solution (50 mL vial). Ultrasonication was carried out using a bath

sonicator (Bandelin Sonorex, 35 kHz). To maintain sonication efficiency and prevent overheating, the water in the bath was decanted and re-filled with fresh water every 30 min. After sonication, samples were left to stand overnight to allow any unstable graphite aggregates to form and then centrifuged (Milipore-amicon MC-13). After centrifugation, the top two-thirds of the dispersion was gently extracted by pipetting.

2.4 Characterization UV-vis absorption spectroscopy was conducted using a Varian Cary 60 spectrophotometer. Optical images were taken using an Olympus BX41 light microscope. Scanning electron microscopy (SEM) observation was carried out using a field emission microscope (FEI Quanta 600 FEG) operated at 20 kV and equipped with an energy-dispersive X-ray spectrometer (EDX). Transmission electron microscopy (TEM) and high-resolution TEM images were recorded with a transmission electron microscope (JEOL 2100F) operated at 200 kV. TEM samples were prepared by pipetting a few milliliters of the dispersion onto holey carbon mesh grids (400 mesh). Raman spectra of graphene films and graphite powder were collected with a Horiba Jobin Yvon LabRam 2 confocal Raman microscope with a HeNe Laser excitation at 633 nm (1.96 eV) with a power of 3.5 mW. Deposited thin films were prepared by vacuum filtration onto porous nylon membranes (Whatman, 0.2 μm pore size, 47 mm membrane diameter) and dried at room temperature. Measurements were taken with 5 s of exposure time using a long working distance objective of 50-fold magnification and aperture 0.5 yielding a beam diameter of ~600 nm in the focus. The peak maximum intensity ratio was obtained by taking the peak intensities following baseline corrections to remove residual fluorescence. Thermogravimetric (TGA) analysis was performed on a Netzsch STA 409 PC/PG instrument in an air atmosphere.

2.5 Thermal conductivity measurements The theoretical background and experimental set-up for thermal conductivity measurements are illustrated in the Supporting Information. The

thermal conductivity sensor was placed in a vessel, which was temperature controlled by a water thermostat (Type C, Haake, Karlsruhe, Germany). In addition, the needle probe was vertically aligned in order to minimize errors related to free convection during the measurement procedure. Moreover, the sensor was connected to one pair of leads for temperature measurements with the type E thermocouple and the other pair supplied the heating current; connected instruments are a data acquisition system (DAQ, 3700 System switch/multimeter equipped with a 3721 multiplex card, Keithley, Munich, Germany) and a constant current source (DC Calibrator J 152, Knick, Berlin, Germany). The junction of the thermocouple and the lead wire were immersed in an ice bath which was used as a 0 °C temperature reference.

Prior to each thermal conductivity measurement, the sample was sonicated for 5 min in an ultrasonic bath (type RK 106, Brandelin electronic, Berlin, Germany). The generated heating power per unit length ($\dot{q}$) was determined from the equation $\dot{q} = \left(R/L\right) \cdot I^2$ using supplied current (I) and the known total resistance per unit length of the heater wire in the sensor (R/L = 1041.5 Ω m^{-1}). The DAQ recorded the temperature course inside the sensor (thermocouple) with an interval of 0.25 s. The thermal conductivity measurements were performed not less than 3 times for each sample at temperatures between 10 and 60 °C with a heating rate of 0.12 W to ensure reproducibility of the experiment. Generated data were analyzed using the maximum slope method according to the literature [20]. This method delivers appropriate thermal conductivity results within an accuracy of 5%.

3. Results and discussion

After being subjected to mild bath sonication followed by centrifugation, stable graphene dispersions in ethanol and isopropanol were obtained in the presence of P20, as clearly seen in the inset of Fig. 1a. The Tyndall effect of the dispersion confirmed its colloidal nature (Fig. S3a).

This contrasts to the settling of graphene flakes upon centrifugation without P20. To find the optimal content of P20 for graphene exfoliation, A_{660}/l was measured for a range of dispersions versus P20 concentration at a fixed $C_{G,I}$ = 5 mg mL^{-1}, which showed a peak at a polymer concentration of 20 mg mL^{-1} (Fig. 1a). As such, we chose to prepare subsequent dispersions with C_{P20} = 20 mg mL^{-1}. The dispersibility of graphene in P20, in terms of A_{660}/l at its optimal concentration, was 4-fold as high as that in NMP. This also surpassed the values in surfactants, such as SC [10] and STC [11], and the polymer PVP [12], each of which was reported to be one of the best dispersing agents. The quantitative comparison of the yield of single-layer graphene by P20, NMP, SC, STC and PVP remains inconclusive at present and needs to be further addressed in our future work. We note that graphene can be readily dispersed in ethanol with the aid of P20, which is not the case using the surfactants. The easy removability of ethanol facilitates further processing of graphene for fabrication of films and composites. Another advantage of using P20 for the exfoliation of graphene is its relatively low toxicity, thus making it more user-friendly than traditional organic solvents and some surfactants or polymers.

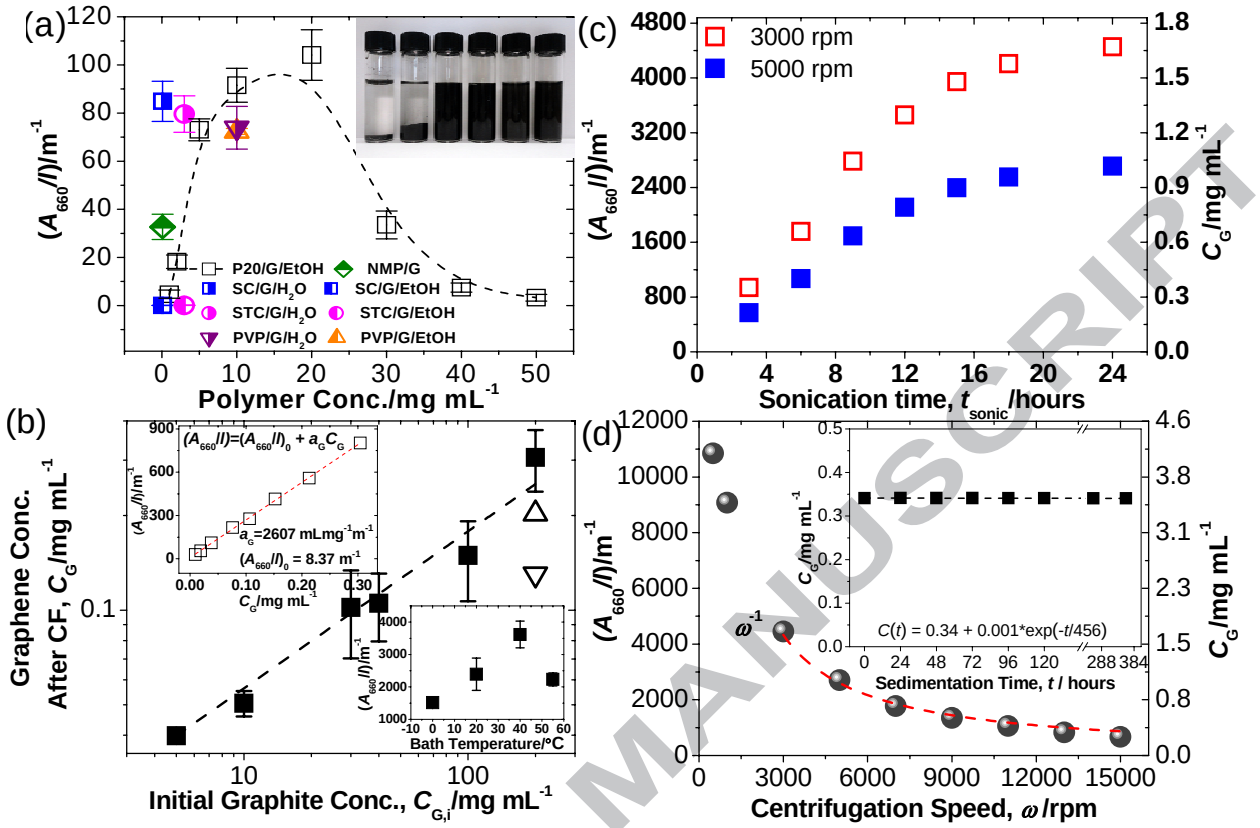

Fig. 1 (a) A_{660}/l, the absorbance per unit-cell-length at 660 nm, for dispersions of graphene (initial graphite concentration $C_{G,I}$ = 5 mg mL^{-1}, t_{sonic} = 1 h, centrifugation: 3000 rpm for 30 min), as a function of C_{P20} in ethanol. For comparison purposes, A_{660}/l data for varying dispersions that were prepared in a similar manner each at its optimal dispersant concentration (SC: 0.1, STC: 3, PVP: 10 mg mL^{-1}) are also shown. Inset: Photographs of dispersions ($C_{G,I}$ = 200 mg mL^{-1}, t_{sonic} = 24 h, centrifugation: 5000 rpm for 30 min); Left to right: G/*i*-PrOH, G/EtOH, P20/G/*i*-PrOH, P20/G/EtOH, and P20/G/*i*-PrOH and P20/G/EtOH both diluted by a factor of 5. (b) Concentration of dispersion (C_G) as a function of $C_{G,I}$. The symbols △ and ▽ represent P08 and P19, respectively. (Insets) Top: A_{660}/l versus C_G. Bottom: A_{660}/l versus sonication bath T. (C_{P20} = 20 mg mL^{-1}, centrifugation: 3000 rpm, 30 min). (c) A_{660}/l versus t_{sonic} for centrifugation speeds of 3000 and 5000 rpm ($C_{G,I}$ = 200 mg mL^{-1}, centrifugation: 30 min). Inset: Absorption spectra

before and after freezing (-26 °C) and heating (70 °C) for 24 h. (d) A_{660}/l versus centrifugation speed ($C_{G,I}$ = 200 mg mL^{-1}, t_{sonic} = 24 h, centrifugation: 30 min). Inset: C_G versus sedimentation time for the dispersion ($C_{G,I}$ = 50 mg mL^{-1}, t_{sonic} = 24 h, centrifugation: 5000 rpm for 30 min). The dashed line in (a) is drawn to guide the eye, whilst the dashed line in either (b) or (d) is the fit to the data shown in the figure.

The UV-vis spectrum of graphene dispersion in P20 is featureless with a monotonic decrease in absorbance with increasing wavelength, except below 320 nm where a strong absorption band is observed which scales with P20 concentration but is less independent on graphene concentration. This band can be mainly ascribed to the P20 (Fig. S4a). Thermogravimetric (TGA) analysis together with knowledge of the mass of (graphitic material + P20) after evaporation of ethanol for known volumes of dispersions allows one to determine the concentration of the stock dispersion. A sample of the stock dispersion was serially diluted with 20 mg mL^{-1} P20 solution. The absorbance per unit-cell-length for each diluted sample was then measured and plotted as a function of graphene concentration (C_G) (top inset, Fig. 1b). A straight line fit through the points gives the absorption coefficient at 660 nm of α = 2607 mL mg^{-1} m^{-1} agreeing reasonably with those reported previously [9,11]. The non-zero intercept in the figure is attributed to the A/l of extra polymer molecules in the dispersion.

Keeping C_{P20} constant at 20 mg mL^{-1}, C_G was measured as a function of $C_{G,I}$ (Fig. 1b). An empirical relationship of $C_G = 0.0178 \times (C_{G,I})^{1/2}$ is observed (t_{sonic} = 1 h, centrifugation: 3000 rpm, 30 min), even at a very high $C_{G,I}$. C_G increases steadily with $C_{G,I}$ and reaches 0.3 mg mL^{-1} at $C_{G,I}$ = 200 mg mL^{-1}, a value that was achieved with SC after over 400 h of bath sonication [10]. We also found that C_G was dependant on sonication temperature and was maximized at 40 °C (bottom inset, Fig. 1b). Moreover, the dispersed concentrations after centrifugation for 30 min at 3000 and 5000 rpm were plotted versus sonication time (t_{sonic}, Fig. 1c). The concentration

increases gradually with t_{sonic}, and attains values of 1.71 and 1.04 mg mL^{-1}, respectively. It was possible to recycle the sediment to increase the yield of graphene further. The concentration after centrifugation at 500 rpm for 90 min (t_{sonic} = 24 h) is as high as ~4 mg mL^{-1}, a value that is much higher than the reported yield using the good surfactant (SC) [10] and the best organic solvent (NMP) [6-7], and even surpasses the results for exfoliation of GO in organic solvents [21]. To the best of our knowledge, this ranks one of the highest concentrations obtained for pristine graphene to date. Significantly, in contrast to 400 h of bath sonication for dispersing graphene in either NMP [7] or SC [10], the processing period herein (24 h) was dramatically reduced. The stabilization of graphene by the polymer may arise from a steric effect, i.e. the hydrophobic polymer segments, which contain a high percentage of allyl methacrylate and butyl acrylate, interact with the surface of graphene, while loops of hydrophilic chains originating from higher amounts of poly (ethylene glycol) methacrylate or dimethylamino methacrylate extend into the bulk ethanol solution, hence preventing the sheets from aggregating.

The concentration after centrifugation at varying centrifugation rates (ω) is shown in Fig. 1d. The C_G value scales well with ω^{-1} at $\geq$ 3000, while an empirical scaling of C_G with the inverse square root of centrifugation time is observed at a fixed centrifugation speed (ω = 5000) (Fig. S4b). The dispersion stability was evaluated by monitoring A_{660}/l and thus concentration as a function of sedimentation time. The profile as shown in the inset of Fig. 1d exhibits an exponential decay and can be well approximated by $c\ (t) = c_0 + (c_T\text{-}c_0)\ e^{-t/\tau}$, where c_0 is the concentration of the stable phase, c_T represents the initial concentration of the dispersion, and τ corresponds to the sedimentation time constant. Fitting the data gave c_0/c_T = 0.997 and τ = 456 h, which indicated that approximately 99.7% of graphene in the dispersion remained stably dispersed against sedimentation over very long times. Moreover, no degradation of the dispersion occurred, even after freezing (–26 °C) or heating (70 °C) for 24 h, which was

reflected by the maintenance of its absorption spectra after subjection to either treatment (Fig. S4c). For a number of applications, water would be the preferred solvent. However, the surface energy of water does not match with that of pristine graphene [6], resulting in a very low yield of graphene in water. With this in mind, it would be of significance to obtain graphene dispersions that can be further processed using water. Here, we found that the P20/G/EtOH dispersions retain high stability against sedimentation for at least 160 h even when exposed to water up to 80% volume ratio, as reflected by the maintenance of the absorbance (Fig. S5A). This may be due to the dissociation of carboxyl groups in the polymer under natural and basic aqueous conditions, which results in effective electrostatic repulsion forces between polymer-coated graphene sheets enabling dispersion stability (Fig. S5B).

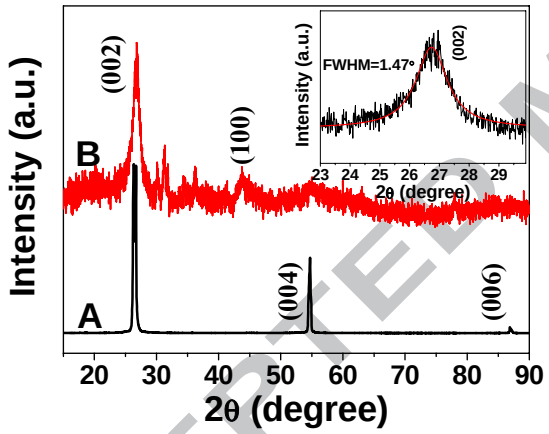

Fig. 2 XRD patterns of the initial graphite and the sample resulting from the P20/G dispersion (t_{sonic} = 24 h, centrifugation: 500 rpm, 30 min) after removal of ethanol at room temperature. Inset: An enlarged (002) reflection with the Lorentzian fit.

Figure 2 shows XRD patterns of the starting graphite and as-obtained P20/G. The diffraction peaks at ~26.8 and ~54.8º in traces A and B originate from the (002) and (004) reflections of the graphitic structure, respectively. The two peaks in trace B are approximately at the same positions as those in trace A, suggesting that the graphite lattice was retained after

exfoliation. However, weakening in the relative intensity of the (004) occurred, and almost no (006) reflection was observed, which concurs with those observed for sublattices consisting of few-layer graphene [22]. A broad peak at ~43.8º appeared corresponding to the (100) plane of graphene. A remarkable broadening of the (002) peak, as shown in trace B, was clearly observed indicating the formation of few-layer graphene. The mean thickness of layers was estimated using the Debye-Scherrer equation: $t=0.89\lambda/B_{(002)}\cos\theta_{(002)}$, where t is the thickness of the graphitic stack and $B_{(002)}$ represents the full width at half maximum (FWHM), which was obtained from the Lorentzian fit for the (002) reflection. The number of layers is thus given by $t/d_{(002)}$ where $d_{(002)}$ corresponds to the interlayer spacing between the (002) planes. In this case, the mean number of layers was calculated to be ~14.

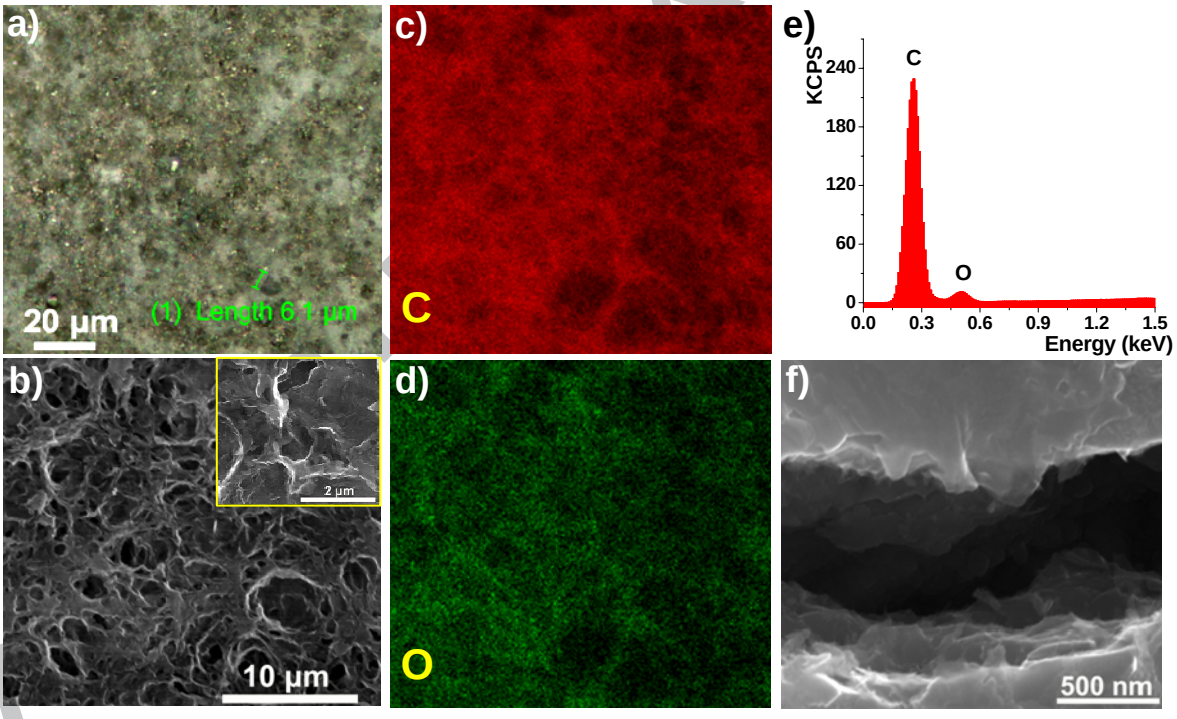

Fig. 3 (a) Optical and (b) SEM images of a deposited sample. Inset in (b): An enlarged SEM image of P20/G showing interconnected graphene sheets. EDX mapping of the region shown in (b): (c) C and (d) O. (e) EDX pattern of the sample shown in (b). (f) SEM image of a crack on

the surface of a film formed by vacuum-filtration of the dispersion.

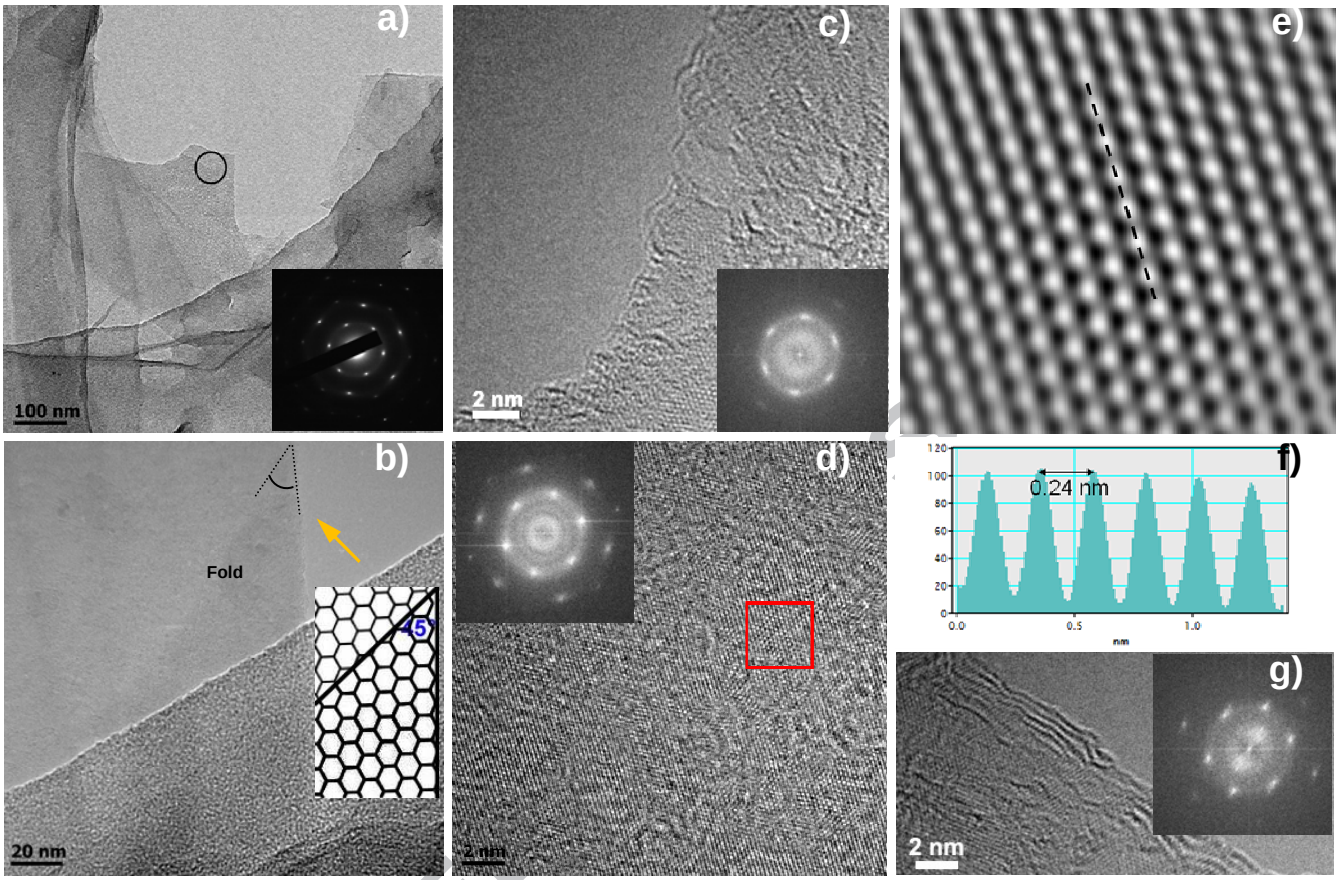

Fig. 4 TEM images of (a) a number of few-layer graphene flakes and (b) an individual thin flake. HRTEM images of (c) a monolayer graphene and (d) a section of monolayer graphene. (e) A filtered image of the region enclosed by the square in (b). (f) Intensity analysis along the dashed line in (e). (g) HRTEM image of a trilayer graphene. The inset in (a) is the FFT of the circled regime. Insets in (c), (d), and (e) correspond to the FFT of the image.

Typical optical microscopy (Fig. 3a), SEM (Figs. 3b, 3f and S6a) along with elemental mapping (Figs. 3c-e), and TEM (Fig. 4a) images show large quantities of graphene-like flakes stabilized by the polymer molecules. In addition to large flakes appearing as dark regions in the optical image, many small flakes with lateral sizes of 500-1.5 μm were detected by TEM. An individual thin flake with possibly a folded morphology is shown in Fig. 4b. Thick multi-layer

sheets were rarely observed, while a significant number of few-layer graphene flakes (less than 5 layers) were easily identified by their edges. Most of the observed flakes appeared to be of good quality and free of holes or other damages. Fig. 4c shows a high-resolution TEM (HRTEM) image of a flake with well-defined edges, that appears to be a monolayer. As observed in the fast Fourier transform (FFT, inset) of the image, intense (1100) spots are seen, whereas the (2110) spots are too weak, further indicative of monolayer graphene. Shown in Fig. 4d is an aberration corrected HRTEM image of a monolayer graphene. A filtered image (Fig. 4e) of the enclosed region shown in Fig. 4d clearly illustrates the hexagonal nature of the graphene. Intensity analysis (Fig. 4f) along the dashed line in Fig. 4e reveals a hexagon width of 0.24 nm, close to the expected value of 0.25 nm [9]. Fig. 4f and Fig. S7f show trilayer and five-layer graphene sheets, respectively.

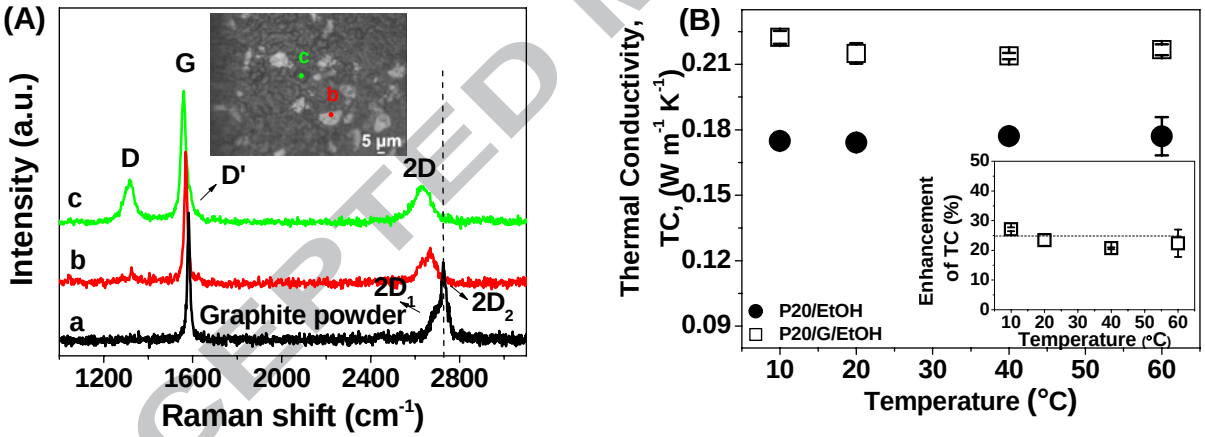

Fig. 5 (A) Raman spectra collected on the regions of large (b) and small (c) flakes for a thin • lm formed by filtration from a dispersion (t_{sonic} = 24 h, centrifugation: 500 rpm, 30 min). Inset: Optical image of the film. Raman mode for the starting graphite is also shown for comparison. (B) Thermal conductivity (TC) of P20/G/EtOH (C_G = 0.055 vol %) and P20/EtOH as a function of temperature. Inset: Enhancement of TC versus temperature.

Figure 5A shows representative Raman spectra of the original graphite powder and thin films formed by vacuum filtration of the graphene dispersions. No D band being associated with the breathing mode of κ-point phonons of A_{1g} symmetry was found in the Raman mode of large flakes. This suggests that the exfoliation process did not lead to the formation of many defects in the graphitic basal plane. The second-order two-phonon-mode 2D band of the flake resembles the 2D band for graphite suggesting that the flake is relatively thick with ≥5 layers. In the case of small flakes, a D band is observed. The ratio of D to G band intensity is about 0.33 which indicates fewer defects than graphene sheets that were produced from the reduction of GO [11]. The Raman spectrum of the flakes is qualitatively in agreement with the Raman spectrum of materials obtained from NMP-based dispersions [6-7]. The 2D line can be described as a single Lorentzian peak possibly indicative of flakes with random stacking. This observation is in contrast to the doublet 2D shape which consists of two components $2D_1$ and $2D_2$ typical of graphite.

An enhancement (≈25%) in thermal conductivity of the P20/G dispersion was observed at a very low volume fraction of 0.055% (Fig. 5B). This outperforms the enhancement of <18% demonstrated for graphene at 0.1 vol% [23] and of 10.5% for both GO and CNT nanofluids at a much higher concentration of 1.0 vol% [24]. The enhancement shows temperature independence akin to GO and CNTs suggesting a percolation model [23]. The superior enhancement of the P20/G nanofluid relates to the low level of defects in the graphene and thus low phonon scattering [25].

4. Conclusions

A set of acrylate polymers was demonstrated to be capable of exfoliating pristine graphite into few-layer graphene in low boiling point alcohols. The polymer showed superior dispersion

ability for graphene compared to the solvent NMP, the surfactants SC and STC, and the polymer PVP. The dispersed concentration increased with the initial graphite concentration and reached significantly high concentrations of up to ~4 mg mL^{-1}. The graphene dispersions showed an enhancement (≈25%) in thermal conductivity at a low graphene volume fraction of 0.055%, suggesting a potential in coolant applications.

Acknowledgments

Zhenyu Sun thanks the Alexander von Humboldt Foundation for financial support.

Supporting Information.

Chemical structures of the polymers, Additional experimental part, TGA, UV, SEM and HRTEM analyses.

References

[1] May P, Khan U, Hughes JM, Coleman J. Role of solubility parameters in understanding the steric stabilization of exfoliated two-dimensional nanosheets by adsorbed polymers. J Phys Chem C 2012;116:11393–400.

[2] Geim AK. Graphene: Status and prospects. Science 2009;324:1530–4.

[3] Stankovich S, Dikin DA, Dommett GHB, Kohlhaas KM, Zimney EJ, Stach EA, et al. Graphene-based composite materials. Nature 2006;442:282–6.

[4] Stankovich S, Dikin DA, Piner RD, Kohlhaas KA, Kleinhammes A, Jia Y, et al. Synthesis of graphene-based nanosheets via chemical reduction of exfoliated graphite oxide. Carbon 2007;45:1558-65.

[5] Sun ZY, Nicolosi V, Rickard D, Bergin SD, Aherne D, Coleman JN. Quantitative evaluation of surfactant-stabilized single-walled carbon nanotubes: Dispersion quality and its correlation with zeta potential. J Phys Chem C 2008;112:10692–9.

[6] Hernandez Y, Nicolosi V, Lotya M, Blighe FM, Sun ZY, De S, et al. High-yield production of graphene by liquid-phase exfoliation of graphite. Nat Nanotechnol 2008;3:563–8.

[7] Khan U, O'Neill A, Lotya M, De S, Coleman JN. High-concentration solvent exfoliation of graphene. Small 2010;6:864–71.

[8] O'Neill A, Khan U, Nirmalraj PN, Boland J, Coleman JN. Graphene dispersion and exfoliation in low boiling point solvents. J Phys Chem C 2011;115:5422–8.

[9] Lotya M, Hernandez Y, King PJ, Smith RJ, Nicolosi V, Karlsson LS, et al. Liquid phase production of graphene by exfoliation of graphite in surfactant/water solutions. J Am Chem Soc 2009;131:3611–20.

[10] Lotya M, King PJ, Khan U, De S, Coleman JN. High-concentration, surfactant-stabilized graphene dispersions. ACS Nano 2010;4:3155–62.

[11] Sun ZY, Masa J, Liu ZM, Schuhmann W, Muhler M. Highly concentrated aqueous dispersions of graphene exfoliated by sodium taurodeoxycholate: Dispersion behavior and potential application as a catalyst support for the oxygen-reduction reaction. Chem --Eur J 2012;18:6972–8.

[12] Wajid AS, Das S, Irin F, Ahmed HST, Shelburne JL, Parviz D, et al. Polymer-stabilized graphene dispersions at high concentrations in organic solvents for composite production. Carbon 2012;50:526–34.

[13] Parviz D, Das S, Ahmed HST, Irin F, Bhattacharia S, Green MJ. Dispersions of non-covalently functionalized graphene with minimal stabilizer. ACS Nano 2012;6:8857–67.

[14] Yang H, Hernandez Y, Schlierf A, Felten A, Eckmann A, Johal S, et al. A simple method for graphene production based on exfoliation of graphite in water using 1-pyrenesulfonic acid sodium salt. Carbon 2013;53**:**357-65.

[15] An XH, Simmons T, Shah R, Wolfe C, Lewis KM, Washington M, et al. Stable aqueous dispersions of noncovalently functionalized graphene from graphite and their multifunctional high-performance applications. Nano Lett 2010;10:4295-301.

[16] Sangermano M, Marchi S, Valentini L, Bon SB, Fabbri P. Transparent and conductive graphene oxide/poly(ethylene glycol) diacrylate coatings obtained by photopolymerization. Macromol Mater Eng 2011;296:401-7.

[17] Saha A, Basiruddin SK, Ray SC, Roy SS, Jana NR. Functionalized graphene and graphene oxide solution via polyacrylate coating. Nanoscale 2010;2:2777-82.

[18] Liao KH, Qian YQ, Macosko CW. Ultralow percolation graphene/polyurethane acrylate nanocomposites. Polymer 2012;53:3756-61.

[19] Pöller S, Beyl Y, Vivekananthan J, Guschin DA, Schumann W. A new synthesis route for Os-complex modified redox polymers for potential biofuel cell applications. Bioelectrochemistry 2012;87:178–84.

[20] Asher GB, Sloan ED, Graboski MS. A computer-controlled transient needle-probe thermal-conductivity instrument for liquids. Int J Thermophys 1986;7:285–94.

[21] Tung VC, Allen MJ, Yang Y, Kaner RB. High-throughput solution processing of large-scale graphene. Nat Nanotechnol 2009;4:25–9.

[22] Shih CJ, Vijayaraghavan A, Krishnan R, Sharma R, Han JH, Ham MH, et al. Bi- and trilayer graphene solutions. Nat Nanotechnol 2011;6:439–45.

[23] Sen Gupta S, Siva VM, Krishnan S, Sreeprasad TS, Singh PK, Pradeep T, et al. Thermal conductivity enhancement of nanofluids containing graphene nanosheets. J Appl Phys 2011;110:084302.

[24] Yu W, Xie HQ, Bao D. Enhanced thermal conductivities of nanofluids containing graphene oxide nanosheets. Nanotechnology 2010;21:055705.

[25] Pop E, Varshney V, Roy AK. Thermal properties of graphene: Fundamentals and applications. MRS Bulletin 2012;37:1273-81.

Captions of figures

Fig. 1 (a) A_{660}/l, for dispersions of graphene (initial graphite concentration $C_{G,I}$ = 5 mg mL^{-1}, t_{sonic} = 1 h, centrifugation: 3000 rpm for 30 min), as a function of C_{P20} in ethanol. For comparison purposes, A_{660}/l data for varying dispersions that were prepared in a similar manner each at its optimal dispersant concentration (SC: 0.1, STC: 3, PVP: 10 mg mL^{-1}) are also shown. Inset: Photographs of dispersions ($C_{G,I}$ = 200 mg mL^{-1}, t_{sonic} = 24 h, centrifugation: 5000 rpm for 30 min); Left to right: G/*i*-PrOH, G/EtOH, P20/G/*i*-PrOH, P20/G/EtOH, and P20/G/*i*-PrOH and P20/G/EtOH both diluted by a factor of 5. (b) Concentration of dispersion (C_G) as a function of $C_{G,I}$. The symbols $\triangle$ and $\triangledown$ represent P08 and P19, respectively. (Insets) Top: A_{660}/l versus C_G. Bottom: A_{660}/l versus sonication bath *T*. (C_{P20} = 20 mg mL^{-1}, centrifugation: 3000 rpm, 30 min). (c) A_{660}/l versus t_{sonic} for centrifugation speeds of 3000 and 5000 rpm ($C_{G,I}$ = 200 mg mL^{-1}, centrifugation: 30 min). Inset: Absorption spectra before and after freezing (-26 °C) and heating (70 °C) for 24 h. (d) A_{660}/l versus centrifugation speed ($C_{G,I}$ = 200 mg mL^{-1}, t_{sonic} = 24 h, centrifugation: 30 min). Inset: C_G versus sedimentation time for the dispersion ($C_{G,I}$ = 50 mg mL^{-}

[1], t_{sonic} = 24 h, centrifugation: 5000 rpm for 30 min). The dashed line in (a) is drawn to guide the eye, whilst the dashed line in either (b) or (d) is the fit to the data shown in the figure.

Fig. 2 XRD patterns of the initial graphite and the sample resulting from the P20/G dispersion (t_{sonic} = 24 h, centrifugation: 500 rpm, 30 min) after removal of ethanol at room temperature. Inset: An enlarged (002) reflection with the Lorentzian fit.

Fig. 3 (a) Optical and (b) SEM images of a deposited sample. Inset in (b): An enlarged SEM image of P20/G showing interconnected graphene sheets. EDX mapping of the region shown in (b): (c) C and (d) O. (e) EDX pattern of the sample shown in (b). (f) SEM image of a crack on the surface of a film formed by vacuum-filtration of the dispersion.

Fig. 4 TEM images of (a) a number of few-layer graphene flakes and (b) an individual thin flake. HRTEM images of (c) a monolayer graphene and (d) a section of monolayer graphene. (e) A filtered image of the region enclosed by the square in (b). (f) Intensity analysis along the dashed line in (e). (g) HRTEM image of a trilayer graphene. The inset in (a) is the FFT of the circled regime. Insets in (c), (d), and (e) correspond to the FFT of the image.

Fig. 5 (A) Raman spectra collected on the regions of large (b) and small (c) flakes for a thin • lm formed by filtration from a dispersion (t_{sonic} = 24 h, centrifugation: 500 rpm, 30 min). Inset: Optical image of the film. Raman mode for the starting graphite is also shown for comparison. (B) Thermal conductivity (TC) of P20/G/EtOH (C_G = 0.055 vol %) and P20/EtOH as a function of temperature. Inset: Enhancement of TC versus temperature.

Supporting Information

High-yield exfoliation of graphite in acrylate polymers: A stable few-layer graphene nanofluid with enhanced thermal conductivity

Zhenyu Sun,*[a] Sascha Pöller,[b] Xing Huang,[c] Dmitrii Guschin,[b] Christoph Taetz,[d] Petra Ebbinghaus,[e] Justus Masa,[b] Andreas Erbe,[e] Andreas Kilzer,[d] Wolfgang Schuhmann,[b] and Martin Muhler[a]

[a] *Laboratory of Industrial Chemistry, Ruhr-University Bochum, D-44780, Bochum, Germany. E-mail: zhenyu.sun@techem.rub.de*

[b] *Analytische Chemie-Elektroanalytik & Sensorik, Ruhr-University Bochum, D-44780, Bochum, Germany*

[c] *Technical Institute of Physics and Chemistry, Chinese Academy of Sciences, Beijing, China*

[d] *Lehrstuhl für verfahrenstechnische Transportprozesse, Ruhr-University Bochum, D-44780, Bochum, Germany*

[e] *Max-Planck-Institut für Eisenforschung GmbH, Max-Planck-Str. 1, 40237 Düsseldorf, Germany*

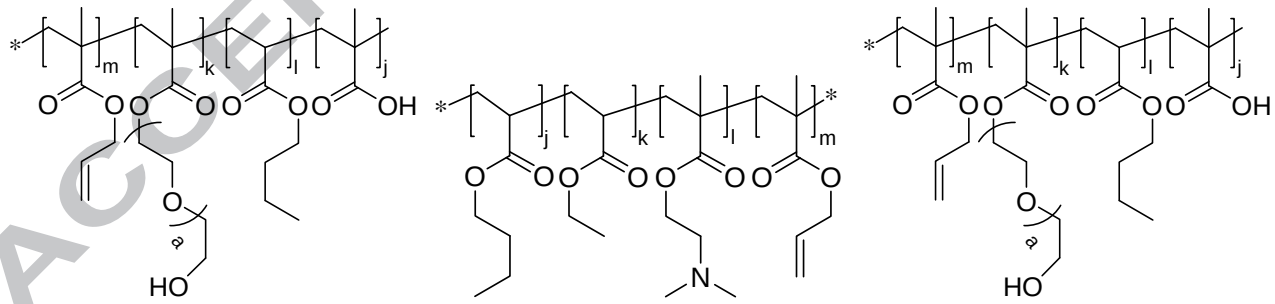

Fig. S1 Chemical structures of the polymers P20, P08 and P19 used in this work.

Table S1 Monomer amounts used for the synthesis of P20, P08, and P19.

	AllMA	PEGMA	BA	DMAEMA	MAA
P20	631 mg / 5.0 mmol	395 mg / 0.75 mmol	417 mg / 3.25 mmol	--	86 mg / 1.0 mmol
P08	631 mg / 5.0 mmol	395 mg / 0.75 mmol	480 mg / 3.75 mmol	79 mg / 0.5 mmol	--
P19	631 mg / 5.0 mmol	395 mg / 0.75 mmol	481 mg / 3.75 mmol	-	43 mg / 0.5 mmol

Theoretical background for thermal conductivity measurements

Thermal conductivity measurements were carried out using a needle probe (sensor) mainly based on the theory of a line heat source [1]. Van der Helden derived a theoretical approach from Fourier's law which can be expressed as follows by assuming an infinite length and a radially symmetric temperature field gradient:

$$\frac{\partial T}{\partial t} = a\left(\frac{\partial^2 T}{\partial r^2} + \frac{1}{r}\frac{\partial T}{\partial r}\right) \qquad \text{Equation 1}$$

where T, t, r, and a correspond to the temperature, time, radius, and thermal diffusivity, respectively. Given a sufficiently long measurement time, ΔT can be approximated as:

$$\Delta T = \frac{\dot{q}}{4\pi\lambda}\left(-\gamma + \ln\left(\frac{4at}{r^2}\right)\right) \quad \text{Equation 2}$$

in which $\dot{q}$ represents the heat flux, λ denotes the thermal conductivity, and γ is Euler's constant (≈ 0.5772) [2]. Furthermore, Equation can be simplified as:

$$\lambda = \frac{\dot{q}}{4\pi}\frac{\ln(t_2) - \ln(t_1)}{T_2 - T_1} \quad \text{Equation 3}$$

This expression was applied here for thermal conductivity determination.

Experimental instrument for thermal conductivity measurements

The sensor (East 30 Sensors, Pullman, USA) used in this work has a diameter of 1.27 mm and a heater length of 60 mm. The length-to-diameter ratio is thus derived as 47.2, a value that is larger than the minimum recommended value of 32 required for the line heat source method [3]. This meets the assumption of an infinitively long and thin heat source. The sensor housing is constructed of a stainless steel tube with a wall thickness of about 0.2 mm, which is filled with highly thermal conductive epoxy (29.7×10^{-4} cal s^{-1} cm^{-1} $°C^{-1}$, given by the manufacturer). The heater wire is made of a temperature invariant resistant evanohm alloy (Ni 75 wt.%, Cr 20 wt.%, Al 2.5 wt.%, Cu 2.5 wt.%). The total resistance per unit length of the heater wire is 1041.5 Ω m^{-1} (provided by the manufacturer). To detect the temperature course during the measurements, a type-E thermocouple is placed in the sensor, the Seebeck coefficient of which is 62 mV K^{-1} [3].

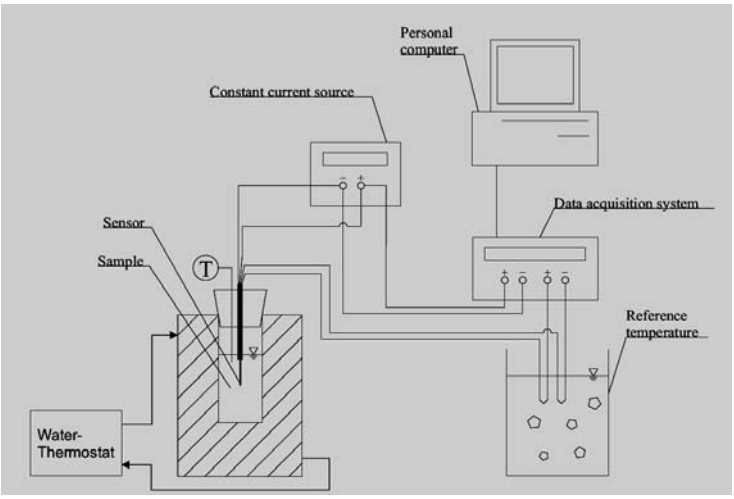

Fig. S2 Experimental set-up of the thermal conductivity apparatus.

The experimental set-up for thermal conductivity measurements is displayed in Fig. S2.

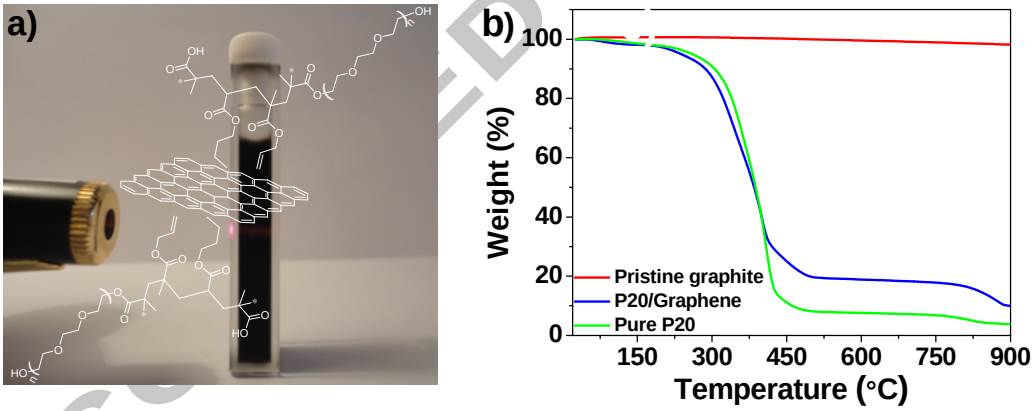

Fig. S3 (a) Photograph of a P20/G dispersion in EtOH. The Tyndall effect of the dispersion confirms its colloidal nature. Inset: Schematic illustration of the stabilization of graphene sheets by polymer molecules through a steric effect, i.e. the hydrophobic polymer segments, which contain a high percentage of allyl methacrylate and butyl acrylate, interact with the surface of graphene while loops of hydrophilic chains, originating from higher amounts of poly (ethylene

glycol) methacrylate or dimethylamino methacrylate, extend into the bulk ethanol solution, thus preventing the sheets from aggregating. (b) TGA thermograms for graphite powder, pure P20, and P20/G obtained with a ramping rate of 10 °C min^{-1} in air.

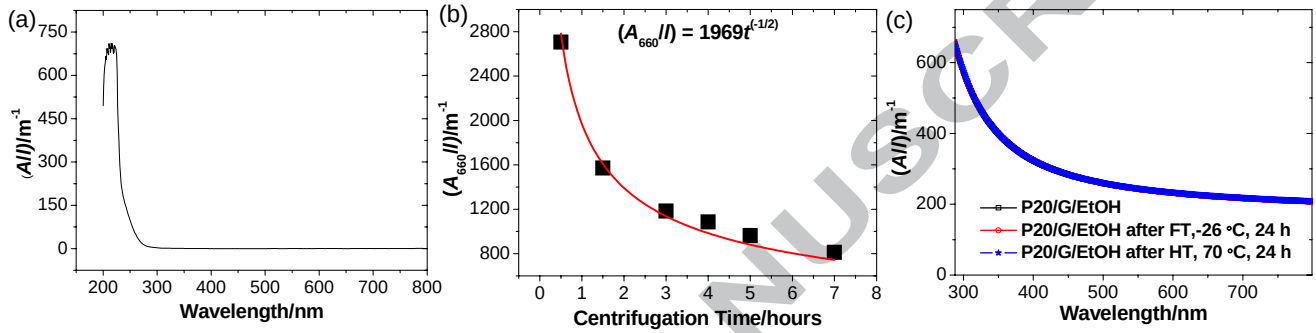

Fig. S4 (a) Absorption spectrum for a P20 ethanol solution at 0.5 mg mL^{-1}. (b) A_{660}/l versus centrifugation time exhibiting an empirical relationship of $A_{660}/l = 1969 \times t^{(-1/2)}$. (c) Absorption spectra before and after freezing (-26 °C) and heating (70 °C) for 24 h.

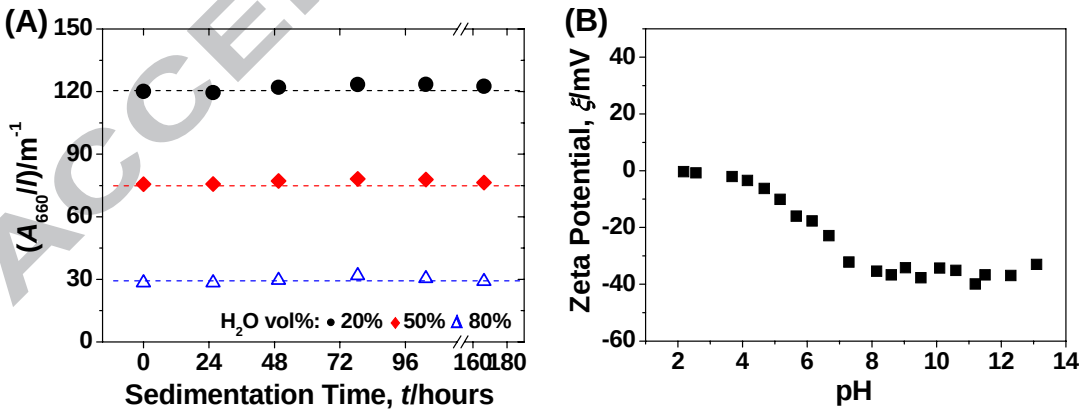

Fig. S5 (A) A_{660}/l versus sedimentation time for graphene dispersions ($C_{G,I}$ = 50 mg mL^{-1}, t_{sonic} = 24 h, centrifugation: 10000 rpm for 1 h) diluted by addition of 20 (●), 50 (♦), and 80% (Δ) H_2O. The dashed lines shown in the figure are drawn to guide the eye. (B) Zeta potentials for the dispersion ($C_{G,I}$ = 50 mg mL^{-1}, t_{sonic} = 24 h, centrifugation: 10000 rpm for 1 h) diluted by addition of 80% H_2O as a function of pH. The absolute values of Zeta potential at original and basic conditions are higher than 30 mV, suggesting the stability of the dispersion. The value decreases with the reduction in pH originating from the neutralization of negative surface charge of polymer-coated graphene sheets.

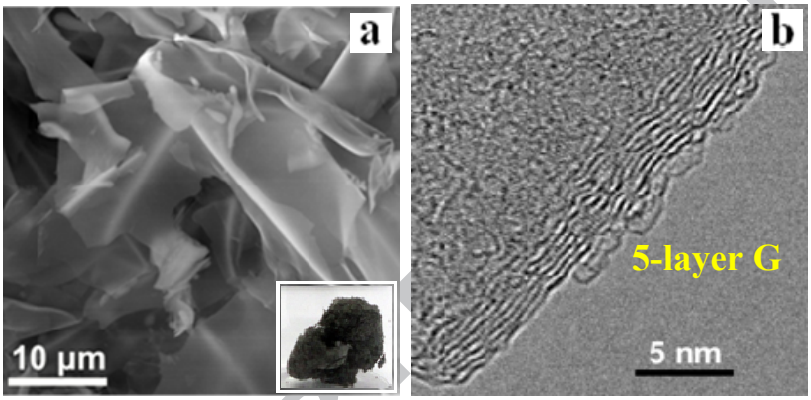

Fig. S6 SEM image of (a) the sample obtained by freeze-drying of the dispersion. Inset in (a) shows the bulk morphology of the freeze-dried sample. (b) HRTEM image of a 5-layer graphene sheet.

[1] Van der Held EFM, Van Drunen FG. A method of measuring the thermal conductivity of liquids. Phys 1949;15:865-881.

[2] Carslaw HS, Jaeger JC. *Conduction of heat in solids*, **1959**, 2nd edition, Oxford, Clarendon Press.

[3] Murakami EG, Sweat VE, Sastry SK, Kolbe E, Hayakawa K, Datta A. Recommended design parameters for thermal conductivity probes for nonfrozen food materials. J Food Eng 1996;27:109-23.